

1 OCT structure, COB location and magmatic type of the Northern
2 Angolan margin from integrated quantitative analysis of deep
3 seismic reflection and gravity anomaly data

4

5 **L Cowie¹, R.M Angelo^{1,2}, N Kuszni¹, G Manatschal³ and B Horn⁴**

6 ¹ Earth and Ocean Sciences, University of Liverpool, Liverpool, L69 3BX, UK

7 ² Presently at ConocoPhillips, Houston, TX 77079, USA

8 ³ CNRS-EOST, Université de Strasbourg, 1 rue Blessing, F-67084 Strasbourg, France

9 ⁴ ION Geophysical / GX Technologies, Houston, Texas, USA

10

11 **Abstract**

12 The crustal structure and distribution of crustal type of the northern Angolan rifted continental
13 margin are greatly debated; hyper-extended continental crust, oceanic crust and exhumed
14 serpentinised mantle have been proposed to underlie the Aptian salt and the underlying sag
15 sequence. Quantitative analysis of deep seismic reflection and gravity anomaly data together with
16 reverse post-breakup subsidence modelling has been used to investigate ocean-continent transition
17 structure, continent-ocean boundary location, crustal type and the palaeo-bathymetry of Aptian salt
18 deposition. Gravity inversion to give Moho depth and crustal thickness, RDA analysis to identify
19 departures from oceanic bathymetry and subsidence analysis shows that the distal Aptian salt is
20 underlain by hyper-extended continental crust rather than exhumed mantle or oceanic crust. We
21 propose that Aptian salt was deposited approximately 0.2km and 0.6km below global sea level and
22 that the inner proximal salt subsided by post-rift (post-tectonic) thermal subsidence alone, while the

23 outer distal salt formed during syn-rift, prior to breakup, resulting in additional tectonic subsidence.
24 Our analysis argues against Aptian salt deposition on the Angolan margin in a 2-3km deep isolated
25 ocean basin, and supports salt deposition on hyper-extended continental crust formed by
26 diachronous rifting migrating from east to west, culminating in late Aptian.

27 **1. Introduction**

28 The northern Angolan rifted continental margin has been the subject of extensive seismic surveys
29 (e.g. Contrucci et al. (2004), Moulin et al. (2005) and Unternehr et al.(2010)). Seismic imaging and
30 interpretation of the sub-salt is difficult due to the presence of thick sedimentary packages which
31 are impacted by a massive middle to upper Aptian salt sequence (up to 5km thickness in places); this
32 presents major scientific and technical challenges to understanding crustal structure and tectonic
33 history. As a result the ocean-continent transition (OCT) structure and continent-ocean boundary
34 (COB) location along the northern Angolan margin are still not fully understood. The presence and
35 distribution of thinned continental crust, oceanic crust and exhumed mantle, the nature of the pre-
36 salt sag basins, the tectonic context of the Aptian salt deposition and whether the salt is pre-
37 breakup or post-breakup, the palaeo-water depths through the breakup period and the mechanisms
38 responsible for the generation of accommodation space are uncertain and much debated (Jackson et
39 al., 2000; Karner and Driscoll, 1999; Karner et al., 2003; Karner et al., 1997; Moulin, 2003; Moulin et
40 al., 2005). In particular there is controversy about whether the salt was deposited in a deep isolated
41 ocean basin or on thinned continental crust.

42 Our analysis along the offshore northern Angolan margin is focussed along three profiles in the
43 Kwanza region; locations are indicated in Figure 1(a). The three profiles include the ION deep long
44 offset seismic reflection profile CS1-2400 (Figure 1(c)), the P3 (Figure 1(d)) and P7+11 profiles (Figure
45 1(e)) (Contrucci et al., 2004; Moulin et al., 2005). The aims of this paper are to determine the OCT
46 structure along the northern Angolan rifted continental margin, to provide an understanding of the

47 palaeo-bathymetries of both proximal and distal base Aptian salt deposition and to examine the
48 location of the salt within the broad framework of the OCT.

49 **2. Integrated Quantitative Analysis Methodology**

50 Integrated quantitative analysis of deep seismic reflection and gravity anomaly data has been
51 applied to the Kwanza margin, offshore northern Angola, in order to determine OCT structure, COB
52 location and magmatic type using ION deep long-offset seismic reflection data. The integrated work-
53 flow and quantitative analytical techniques, which have been applied, consist of: gravity anomaly
54 inversion, residual depth anomaly (RDA) analysis and subsidence analysis. The combined
55 interpretation of these independent quantitative measurements is used to determine OCT structure,
56 COB location and margin magmatic type. This integrated approach has been validated on the
57 Iberian margin (Cowie, 2015) where ODP drilling provides ground-truth of OCT crustal structure, COB
58 location and magmatic type. In addition, we apply a joint inversion technique, using deep seismic
59 reflection and gravity anomaly data, to determine the lateral variation of crustal basement density
60 and seismic velocity for the ION deep seismic reflection profile CS1-2400. The joint inversion of deep
61 seismic and gravity data provides validation of crustal basement thickness interpreted from deep
62 long-offset seismic reflection data and is used to help further constrain crustal basement type.

63 **2.1. Crustal basement thickness and continental lithosphere thinning from gravity** 64 **anomaly inversion**

65 Gravity anomaly inversion has been used to determine Moho depth, crustal basement thickness, and
66 continental lithosphere thinning factors ($1 - 1/\beta$). The data used within our gravity anomaly inversion
67 are bathymetry (Amante and Eakins, 2009) (Figure 1(a)), satellite derived free air gravity (Sandwell
68 and Smith, 2009) (Figure 1(b)), 2D sediment thickness from pre-stacked depth migrated (PSDM)
69 seismic reflection data along CS1-2400 profile (Figure 1(c)) and ocean age isochrons from Müller et
70 al. (1997). The gravity anomaly inversion methodology is described in Chappell and Kusznir (2008)

71 and Greenhalgh and Kuszniir (2007) and has been applied in Cowie and Kuszniir (2012) and Alvey et
72 al. (2008).

73 The gravity anomaly inversion method is carried out in the 3D spectral domain, using the scheme of
74 Parker (1972) and also incorporates a lithosphere thermal gravity anomaly correction, which
75 accounts for the lithosphere mass deficiency due to the elevated geothermal gradient within
76 oceanic and thinned continental margin lithosphere. Without the inclusion of the lithosphere
77 thermal gravity anomaly correction at rifted continental margins, predicted Moho depth and crustal
78 basement thickness are too thick and continental lithosphere thinning factors are too low. The
79 thermal gravity anomaly correction is dependent on the thermal re-equilibration time since
80 lithosphere stretching and thinning, and therefore on continental breakup age. There is general
81 agreement (e.g. Karner and Gambôa (2007) and Aslanian et al.(2009)) that rifting on the Angolan
82 margin started in the Neocomian and culminated with continental breakup in the late Aptian.
83 However, there is no consensus on the rates of lithosphere stretching and thinning through this time
84 interval, although there is some evidence that deformation rates accelerated in the Barremian and
85 Aptian (e.g. Crosby et al. (2011)). While a finite rifting model would be appropriate to determine the
86 lithosphere thermal anomaly developed during lithosphere stretching and thinning leading to
87 breakup, the history of rifting rates is not known. As a consequence we use an instantaneous rift
88 model to determine lithosphere thermal perturbation and explore upper and lower bounds of rift
89 age. We have used 112Ma, corresponding to the age of breakup, after Moulin (2005), for the
90 preferred thermal re-equilibration time to determine the lithosphere thermal gravity anomaly
91 correction, but have also examined sensitivities to ages for thermal re-equilibration which span the
92 period Berriasian (140Ma) to early Albian (110Ma). This range corresponds to the start and end of
93 the main rifting episode in the South Atlantic (Teisserenc and Villemin, 1989).

94 Gravity anomaly inversion Moho depths have been calibrated against seismic Moho depths from the
95 oceanic domain of the CS1-2400 profile using the clear Moho reflectors. Calibration suggests that a

96 reference Moho depth of 35.5km is required in order to predict crustal basement thicknesses
97 consistent with those seen in the oceanic domain of the CS1-2400 seismic reflection profile. An
98 uncertainty in the oceanic Moho depth on the CS1-2400 PSDM depth section, used for the
99 calibration of reference Moho depth, arises from uncertainty in basement seismic velocity but is
100 estimated to be no more than +/- 0.5km.

101 A crustal cross section along the CS1-2400 profile (Figure 2(a)) has been constructed using Moho
102 depths predicted from gravity anomaly inversion assuming the calibrated reference Moho depth of
103 35.5km; bathymetry and 2D sediment thickness are from the CS1-2400 seismic profile. The crustal
104 cross section highlights changes in crustal basement thicknesses along the CS1-2400 profile. At the
105 western end of the profile the gravity anomaly inversion predicts crustal basement thicknesses
106 between 5km and 7km; in the central region of the profile crustal basement thicknesses thicken to
107 approximately 11km and at the eastern end of the profile the crustal basement thickens to
108 approximately 25km. Moho depths determined from the gravity anomaly inversion are generally in
109 good agreement with those seen on the CS1-2400 seismic profile.

110 The corresponding continental lithosphere thinning factor ($\gamma=1-1/\beta$) estimates for profile CS1-2400,
111 derived from gravity anomaly inversion, assuming depth uniform stretching and thinning are shown
112 in Figure 2(b). Continental lithosphere thinning factors of zero indicate that there has been no
113 stretching or thinning of the continental lithosphere, whereas a continental lithosphere thinning
114 factor of one indicates that there has been infinite stretching and thinning of the original continental
115 lithosphere and that no continental crust or lithosphere remains. Stretching of continental
116 lithosphere leads to a decrease in crustal basement thickness; however, decompression melting
117 during rifting and seafloor spreading generates oceanic crust, SDRS (seaward dipping reflectors) and
118 magmatic underplating, which increases crustal basement thickness. A correction for magmatic
119 addition has been included within the gravity anomaly inversion method, and uses a
120 parameterization of the decompression melting model of White and McKenzie (1989) to predict the

121 thickness of the crustal magmatic addition (see Chappell & Kusznir (2008)). Decompression melting
122 and the resulting volume and timing of magmatism during rifting and continental breakup is
123 sensitive to the thermal structure of the continental lithospheric and asthenospheric mantle, its
124 chemical composition (enriched or depleted), the rate of lithosphere stretching and thinning, and
125 the amount of melt retention within the mantle. As a consequence we do not believe that it is
126 possible to apply a deterministic approach to the prediction of magmatic addition. Instead we
127 examine two end members; normal magmatic addition and magma-starved. A 'normal' magmatic
128 solution corresponds to 'normal' decompressional melting that predicts a 7km thick oceanic crust,
129 which is initiated at a critical thinning factor of 0.7. In our magma-starved solution, there is no
130 magmatic addition from decompression melting.

131 The distribution of continental lithosphere thinning factors can be used to help constrain OCT
132 structure and COB location along the profile. At the western end of the profile the continental
133 lithosphere thinning factors for a 'normal' magmatic solution are 1.0 whilst for a magma-starved
134 solution the continental lithosphere thinning factors are approximately 0.85. In the central section
135 of the profile, the continental lithosphere thinning factors, for both solutions examined, reduce to
136 between 0.7 and 0.85. At the western end of the profile we prefer the normal magmatic solution;
137 however, in the central and eastern region of the profile we believe that the magma-starved
138 solution is preferential.

139 Using an older age of 140Ma for the age of lithosphere thermal perturbation (and thermal
140 relaxation) reduces the magnitude of the lithosphere thermal gravity anomaly correction. As a
141 consequence this gives a slightly deeper Moho, thicker crust and lower thinning factors for the
142 central and eastern part of the profile. This sensitivity to rift age is relatively minor and does not
143 affect the interpretation of OCT structure or crustal type.

144 2.2. Residual depth anomaly (RDA) analysis along the CS1-2400 profile

145 RDA analysis has been applied to examine OCT bathymetric anomalies with respect to expected
146 oceanic bathymetries along the CS1-2400 profile (Figure 3). RDAs are commonly used for oceanic
147 regions to compare observed bathymetry with that predicted from secular cooling models of oceanic
148 lithosphere. A RDA, for oceanic crust, is the difference between observed bathymetry (b_{obs}) and
149 bathymetry predicted from ocean age ($b_{predicted}$).

$$150 \quad RDA = b_{obs} - b_{predicted} \quad (1)$$

151 Zero oceanic RDAs correspond to oceanic crust of global average thickness (7 km) in the absence of
152 mantle dynamic topography; positive RDAs correspond to thicker than average oceanic crust, and
153 negative RDAs to thin oceanic crust or serpentinised exhumed mantle. We determine RDAs for the
154 CS1-2400 profile in order to investigate where the RDA signal varies from that seen in the oceanic
155 domain due to changes in crustal thickness and composition across the ocean-continent transition.
156 The age of the lithosphere thermal perturbation due to rifting and breakup in the ocean-continent
157 transition, and its thermal re-equilibration time, correspond to the breakup age and the age of the
158 oldest oceanic lithosphere.

159 Age predicted bathymetric anomalies have been calculated from Crosby and McKenzie (2009). The
160 age of oceanic lithosphere is taken from the global ocean isochron model of Müller et al. (2008). The
161 region inboard of the oldest ocean isochron (corresponding to the breakup age) may be given that
162 age or the isochron gradient may be projected into the margin. The difference in the predicted RDA
163 between these two approaches to defining the thermal age of the continental margin lithosphere is
164 negligible and has no impact on the RDA interpretation. Sensitivities to the thermal plate model
165 predictions from Parsons and Sclater (1977) and Stein and Stein (1992) have also been examined;
166 RDA results computed using these different thermal plate model predictions do not differ
167 significantly.

168 RDAs have been corrected for sediment loading. Present day bathymetry is corrected for sediment
169 loading using flexural backstripping and decompaction (Kusznir et al., 1995) which comprises the
170 removal of the sedimentary load, allowing for the flexural isostatic response and decompaction of
171 the remaining sediments. Flexural backstripping and decompaction assumes shaly-sand compaction
172 and density (Sclater and Christie, 1980) during the removal of the sedimentary layer, whilst the salt
173 layer is given a simple salt lithology (Hudec and Jackson, 2007). Figure 3(b) shows a comparison of
174 the uncorrected RDA and the sediment corrected RDA along the CS1-2400 profile (Figure 3(a)). At
175 the western end of the profile there is approximately a 1500m difference between the uncorrected
176 RDA and the sediment corrected RDA, the largest difference is seen in the central section of the
177 profile. The sediment corrected RDA along the CS1-2400 profile (Figure 3(b)), is positive with a
178 magnitude between zero and +300m at the western end of the profile.

179 The sediment corrected RDA has a minor sensitivity to the effective elastic thickness used during
180 flexural backstripping to define flexural isostatic response to the sediment unloading correction. We
181 use an effective elastic thickness of 1.5km which is appropriate for the shorter wavelength syn-rift
182 sediment loads (see Roberts et al. (1998) for further discussion).

183 **2.3. Continental lithosphere thinning from subsidence analysis along the CS1-2400** 184 **profile**

185 Subsidence analysis has been used to determine the distribution of continental lithosphere thinning
186 and the distal extent of continental crust in order to constrain OCT structure. Subsidence analysis
187 involves the conversion of water loaded subsidence into continental lithosphere thinning factors,
188 assuming McKenzie (1978). Water loaded subsidence, determined by flexural backstripping, is
189 interpreted as the sum of initial (S_i) and thermal (S_t) subsidence in the context of the McKenzie
190 (1978) intra-continental rift model. A correction for magmatic addition due to adiabatic
191 decompression (White and McKenzie, 1989) during continental rifting and seafloor spreading has
192 been included (see Roberts et al. (2013)) and uses the same scheme as described earlier in the

193 gravity anomaly inversion methodology. Magmatic addition from decompression melting increases
194 the thickness of the crust thinned by lithosphere stretching due to intrusion and extrusion, which
195 isostatically reduces the initial subsidence as predicted by McKenzie (1978) and corresponds to the
196 formation of oceanic crust.

197 Figure 4(b) shows sensitivities to continental lithosphere thinning factors from subsidence analysis,
198 including a 'normal' magmatic solution, and a magma-starved solution, with reference to the CS1-
199 2400 profile (Figure 4(a)). At the western end of the profile a 'normal' magmatic solution predicts
200 thinning factors of 1.0 whilst a magma-starved solution predicts thinning factors of approximately
201 0.9.

202 **2.4. Joint inversion of deep seismic and gravity anomaly data: application to the CS1-** 203 **2400 profile**

204 Joint inversion of deep seismic reflection and gravity anomaly data has been applied to the CS1-2400
205 profile in order to both (i) validate the seismic interpretation of Moho and to (ii) determine the
206 lateral variation in crustal basement density and seismic velocity. The ION deep seismic profile has
207 been interpreted in both the time (PSTM) and depth (PSDM) domain. The joint inversion process
208 requires that the seismic reflection data shows seismic reflectivity from the Moho; for the CS1-2400
209 profile this corresponds to most of the section apart from beneath the thick distal salt.

210 Moho depth is first determined from gravity inversion, as described in section 2, using sediment
211 thicknesses from the PSDM depth section.. The crustal basement thickness determined from gravity
212 inversion is converted to interval two-way travel time and then added to the seismic interpretation
213 of top basement on the PSTM time section to show the gravity Moho in the time domain. The
214 basement seismic velocity V_p used for this conversion from interval depth to interval two-way travel
215 time is calculated from the crustal basement density used in the gravity inversion using the empirical
216 linear relationship proposed by Birch (Birch, 1964; Ludwig et al., 1970). The initial value of basement
217 density used in the gravity inversion is 2850 kgm^{-3} (Chappell and Kusznir, 2008). Because the

218 comparison of the gravity Moho depth with the seismic reflection image is carried out in the time
219 domain, the joint inversion methodology is not affected by uncertainties in the basement seismic
220 velocities used to produce the PSDM depth seismic image.

221 The gravity inversion Moho for CS1-2400, converted into the time domain, is shown in Figure 5(a)
222 superimposed on the PSTM section. The seismic interpretation of Moho two-way travel time and the
223 gravity Moho depth taken into the time domain compare well. This suggests that the seismic
224 interpretation of Moho on the PSTM section is correct and validates the deep seismic interpretation.

225 The differences in two-way travel time between the seismic and gravity Mohos is assumed to arise
226 from heterogeneity in crustal basement density and seismic velocity. The joint inversion solves for
227 coincident seismic and gravity Moho in the time domain and calculates the lateral variation of
228 crustal basement density and seismic velocity along profile (Figure 5(c) & (d)). The joint inversion is
229 carried out using the time domain (PSTM) seismic reflection data, as this is the raw data and does
230 not have the assumed basement seismic velocities of the depth domain (PSDM) seismic sections.

231 Joint inversion determines the combination of basement seismic velocities and densities required,
232 along the profile, in order to match the Moho predicted from gravity anomaly inversion to the
233 picked Moho, in the time domain. Basement density and seismic velocity are assumed to be linked
234 by Birch's empirical relationship (Birch, 1964). During the joint inversion, changes in basement
235 density change the Moho predicted from gravity anomaly inversion in the depth domain;
236 corresponding changes in seismic velocity change the conversion of the new gravity Moho from the
237 depth domain into the time domain.

238 Basement densities and seismic velocities from the joint inversion, shown in Figure 5(c and d), show
239 lateral variations along profile. The basement densities and seismic velocities for the western distal
240 end of the CS1-2400 profile are significantly higher than those for the remaining profile. We suggest
241 that the higher values in the west correspond to oceanic crustal basement while the lower values in

242 the centre and east correspond to continental crustal basement. The short wavelength variations in
243 basement density and seismic velocity arise from the inversion methodology and result from fault
244 controlled top basement topography.

245 Solving for the coincident seismic and gravity anomaly inversion predicted Moho in the time domain
246 gives an improved estimate of Moho depth. This improved estimate from joint inversion is shown in
247 Figure 5(b) and compared with that derived from gravity inversion alone.

248 **3. OCT structure and COB location along the CS1-2400 profile**

249 Within the literature there are a range of different definitions of the OCT and COB (e.g. Péron-
250 Pinvidic et al. (2007), Whitmarsh and Miles (1995), Manatschal et al. (2001), Dean et al. (2000)
251 Manatschal et al. (2010) and Discovery 215 Working Group (1998). Within this paper, we define the
252 OCT as the region between unequivocal continental crust of 'normal' thickness and unequivocal
253 oceanic crust; the lithosphere in this region is highly thinned, with complex tectonics, variable
254 magmatism and possible mantle exhumation. We define the COB as the distal limit of unequivocal
255 continental crust; however, determining the location of the COB is made difficult by the presence of
256 exhumed mantle and complex tectonics.

257 A composite analysis plot for profile CS1-2400 is shown in Figure 6, consisting of (a) crustal cross
258 section from gravity anomaly inversion, (b) comparison of the sediment corrected RDA and the RDA
259 component from crustal thickness variations (RDA_{CT}), (c) comparison of the continental lithosphere
260 thinning factors predicted from gravity anomaly inversion and subsidence analysis (d) lateral
261 variations in basement density and (e) seismic velocity from joint inversion. The joint inversion
262 results, including Moho depth, crustal basement densities and seismic velocities have been
263 'smoothed' by computing a moving average, using a spatial gate of 30km.

264 Due to the thick sedimentary cover and mobile salt (including salt diapirs and canopies), seismic
265 imaging of the salt and pre-salt sedimentary units is difficult, which could lead to errors in our

266 interpretation of the internal structure and thickness of the salt and the pre-salt sedimentary layers.
267 We are however, more confident in our pick of the base salt. In order to understand the
268 implications of either over or under estimating the thickness of the salt layer we have examined the
269 effect of treating the salt layer as a sedimentary layer with a shaly sand lithology within the gravity
270 inversion; this results in a slightly deeper Moho and smaller continental lithosphere thinning factors
271 from the gravity inversion. The inclusion or omission of the salt layer does not fundamentally
272 change our interpretation of the crustal domains along the profile.

273 The composite analysis plot is interpreted as showing three distinct crustal zones along the CS1-2400
274 profile highlighted by the dashed lines: zone A – oceanic crust, zone B – hyper-extended continental
275 crust and zone C – continental crust. The dashed lines indicate the boundaries between each of
276 these interpreted crustal domains; although these interfaces are shown as a sharp line, in reality
277 they are likely to be transitional boundaries. The COB is identified as the ocean-ward start of
278 ‘normal’ oceanic crust and is identified by changes in crustal basement thickness, inflections in the
279 RDA analysis signals and also changes in the continental lithosphere thinning from subsidence
280 analysis and gravity anomaly inversion.

281 *Zone A - Oceanic crust*

282 In zone A, the crustal basement thicknesses (Figure 6(a)) predicted from gravity anomaly inversion
283 range between 5km and 6km, as expected for oceanic crust. Oceanic crust of normal thickness
284 should have a sediment corrected RDA of approximately zero, notwithstanding the contribution of
285 mantle dynamic topography. The sediment corrected RDA in this domain (Figure 6(b)) is slightly
286 positive, consistent with the presence of oceanic crust together with some mantle dynamic uplift;
287 this is in agreement with the mantle dynamic uplift reported by Crosby & McKenzie (2009) for the
288 Angolan margin. In addition to the RDA corrected for sediment loading, the RDA component from
289 variations in crustal basement thickness (RDA_{CT}) has also been computed, which is the result of the

290 presence of anomalously thick or thin crust. In this domain the RDA_{CT} is negative, which implies that
291 the crustal basement is thinner than 7km, which is in agreement with the crustal basement
292 thicknesses predicted from gravity inversion. The continental lithosphere thinning factors predicted
293 from gravity anomaly inversion and subsidence analysis are in good agreement (Figure 6(c)) and
294 predict continental lithosphere thinning factors of 1.0, for a 'normal' magmatic solution, implying
295 the presence of oceanic crust. Joint inversion of deep seismic and gravity data calculates crustal
296 basement densities for zone A which range between 2850kgm^{-3} and 3035kgm^{-3} (with an average
297 basement density of approximately 2940kgm^{-3}) (Figure 6(d)) and seismic velocities, which range
298 between 6.7kms^{-1} and 7.1kms^{-1} (Figure 6(e)). These basement densities (and corresponding seismic
299 velocities) are larger than the crustal basement density (2850kgm^{-3}) used within the initial gravity
300 anomaly inversion, which is to be expected as typical oceanic crustal densities range between
301 2860kgm^{-3} and 2900kgm^{-3} (Carlson and Herrick, 1990; Carlson and Raskin, 1984; Fowler, 2006).

302 Between the oceanic domain and the hyper-extended continental crust domain, we interpret a
303 domain of transitional crust; we believe that the crust is a mix of hyper-extended continental crust
304 and magmatic addition. We interpret the edges of this transitional region as the inner and outer
305 bounds of the COB. Within this region we see an increase in crustal basement thickness and both
306 the sediment corrected RDA and the RDA_{CT} , whilst the continental lithosphere thinning factors
307 decrease. At the western end of the hyper-extended continental crust domain, the thinning of the
308 continental crust may increase together with the start of magmatic addition as ocean crust is
309 approached. Our interpretation of the presence of hyper-extended continental crust with the
310 presence of magmatics in this region is significantly different to that proposed by Unternehr et al.
311 (2010), who proposes the presence of serpentinized exhumed mantle. Our quantitative analysis
312 results show no evidence of exhumed mantle; exhumed mantle would show a thinner crust from
313 gravity inversion, negative sediment corrected RDAs and higher continental lithosphere thinning
314 factors.

315 *Zone B - Hyper-extended continental crust*

316 In our interpreted hyper-extended continental crust domain, gravity anomaly inversion predicted
317 crustal basement thicknesses range between 7km and 12km (Figure 6(a)). Both the sediment
318 corrected RDA and the RDA_{CT} (Figure 6(b)) plateau in this domain, at approximately 1000m for the
319 sediment corrected RDA and at approximately 500m for the RDA_{CT} . The continental lithosphere
320 thinning factors from gravity anomaly inversion and subsidence analysis are in good agreement in
321 zone B (Figure 6(c)) and range between 0.7 and 0.85, which is indicative of thinned continental crust.
322 Basement densities and seismic velocities, predicted from joint inversion, are less than those
323 calculated in zone A, the basement densities range between approximately 2800kgm^{-3} and 2900kgm^{-3}
324 (Figure 6(d)) and the corresponding seismic velocities range between 6.5kms^{-1} and 6.75kms^{-1}
325 (Figure 6(e)).

326 *Zone C - Continental crust*

327 At the eastern end of the profile we interpret continental crust as the crustal basement thickness
328 and both the sediment corrected RDA and RDA_{CT} increase, whilst the continental lithosphere
329 thinning factors decrease to between 0.2 and 0.4. The predicted basement densities range between
330 2800kgm^{-3} and 2855kgm^{-3} and the seismic velocities range between 6.5kms^{-1} and 6.8kms^{-1} . The
331 average basement density for zone C is approximately 2830kgm^{-3} , which is within the range
332 proposed for the density of continental crust (Carlson and Herrick, 1990; Christensen and Mooney,
333 1995; Le Pichon and Sibuet, 1981) and is similar to that used within the initial gravity anomaly
334 inversion (2850kgm^{-3}). Zone C includes the margin necking zone.

335 **4. Palaeo-bathymetry of the base Aptian salt deposition from reverse post-**
336 **breakup thermal subsidence modelling**

337 The palaeo-bathymetry of the base Loeme salt (top Aptian) deposition on the Angolan rifted
338 continental margin has been determined using reverse post-breakup subsidence modelling (Kusznir

339 et al., 1995; Roberts et al., 1998). We have focussed on the CS1-2400 profile, but have also looked
340 at two further profiles to the north, P3 and P7+11 profiles (Contrucci et al., 2004; Moulin et al.,
341 2005). Reverse post-breakup subsidence modelling consists of the sequential flexural isostatic
342 backstripping of the post-breakup sedimentary sequences, decompaction of the remaining
343 sedimentary units and reverse modelling of post-breakup lithosphere thermal subsidence. The
344 magnitude of continental lithosphere stretching factor (β) (McKenzie, 1978) which we predict from
345 gravity anomaly inversion controls the amount of reverse post-breakup thermal subsidence and
346 hence the restored model elevation relative to sea level and the predicted palaeo-bathymetry
347 (Roberts et al., 2009; Roberts et al., 1998).

348 Flexural backstripping and decompaction has been applied to the CS1-2400 profile (Figure 7(a)) to
349 remove the salt and post-salt sedimentary layers in order to determine the bathymetry corrected for
350 sedimentary loading to base salt (Figure 7(b)). The complex salt movement in this region may
351 appear to be problematic for flexural backstripping. However, within the palaeo-bathymetric
352 restoration we use the base salt as the target surface for backstripping, which allows us to ignore the
353 salt movement, as we flexurally backstrip through the salt to the time of deposition. We are able to
354 disregard the salt movement because as the salt moved the lithosphere would have responded
355 isostatically to compensate.

356 Flexural backstripping and decompaction gives an incomplete palaeo-bathymetric restoration of
357 base salt; we also need to include reverse post-breakup thermal subsidence. We determine the
358 magnitude of reverse post-breakup thermal subsidence by the continental lithosphere thinning
359 factor ($\gamma=1-1/\beta$) derived from gravity anomaly inversion. Lithosphere thinning factors from gravity
360 inversion are shown in Figure 7(c) assuming a 112Ma rift age for the thermal gravity anomaly
361 correction in the gravity inversion; sensitivities for a normal magmatic solution and a magma-starved
362 solution have been examined. As discussed in previous sections the continental lithosphere thinning
363 factors for a normal magmatic solution are 1.0 at the western end of the CS1-2400 profile; whereas

364 for a magma-starved solution, the continental lithosphere thinning factors are approximately 0.85.
365 In the central section of the profile, the continental lithosphere thinning factors are between 0.7 and
366 0.85 for both solutions examined.

367 Figure 7(d) shows the restored palaeo-bathymetry to base salt, including reverse thermal subsidence
368 modelling, assuming a normal magmatic solution and a breakup age of 112Ma. The proximal base
369 salt restores to just below global sea level with an average bathymetry of approximately 0.2km. In
370 contrast, the distal base salt does not restore to near sea level; restored palaeo-bathymetries for the
371 distal base salt (smoothing through fault controlled topography) are between approximately 0.9km
372 and 2.5km below global sea level. In the deep fault controlled troughs, palaeo-bathymetries for the
373 distal base salt of approximately 4.0km below sea level are predicted.

374 The restored palaeo-bathymetry to base salt, assuming a magma-starved solution (Figure 7(e)), also
375 shows that the proximal base salt restores to approximately 0.2km below global sea level, whilst the
376 distal base salt again does not. The predicted palaeo-bathymetries of the distal base salt range
377 between approximately 0.9km and 3km below sea level (smoothing through fault controlled
378 topography); in the deep structural troughs the palaeo-bathymetries are greater (approximately
379 4.5km below sea level).

380 We believe that the normal magmatic addition solution (Figure 7(d)) is applicable to the oceanic part
381 of the profile whilst the magma-starved solution (Figure 7(e)) is more applicable to the continental
382 end of the profile, with a transitional region in between. In the oceanic domain, water depths at
383 breakup of approximately 2.5km (± 0.2 km depending on magmatic solution), consistent with a young
384 oceanic ridge are predicted, for both a normal magmatic and a magma-starved solution.

385 Rifting on the Angola margin is believed to have commenced in the Neocomian (Teisserenc and
386 Villemin, 1989). For the inner margin, beneath the proximal salt, the main rifting event may have
387 been in the Barremian (Crosby et al., 2011). If a rift age of 130Ma is used to give the lithosphere

388 thermal correction in the gravity inversion and in the reverse post-breakup subsidence modelling,
389 then the proximal base salt restores to approximately 0.6km below global sea-level. There still
390 remains a substantial difference between the restored bathymetry of base proximal and distal salt.

391 As discussed earlier it is possible that our interpretation has overestimated the thickness of the distal
392 salt. We have examined the effect of treating the salt layer as a sedimentary layer within the gravity
393 inversion and the reverse post-breakup subsidence modelling. Reducing the thickness of the salt has
394 a negligible effect on the predicted bathymetry of both proximal and distal salt.

395 An additional sensitivity to the continental lithosphere thinning factors, used to drive reverse
396 thermal subsidence, has been examined along the CS1-2400 profile. A continental lithosphere
397 thinning factor of 1.0 (corresponding to $\beta=\infty$), which gives an upper bound of the restored post-
398 breakup thermal subsidence, has been applied to the entire profile. The predicted bathymetry for
399 the distal base salt remains almost unchanged at between 2km and 3km below global sea level. This
400 implies that, if the distal base salt was deposited at or just below global sea level, it has subsided not
401 only due to post-breakup thermal subsidence and sediment loading.

402 The location of the outer (or more distal) interpreted COB, determined from integrated quantitative
403 analysis, is identified, by the dashed line on Figure 7, in order to examine where the salt is located
404 within the OCT. We believe that the majority of the salt along the CS1-2400 profile is located to the
405 east of the COB on hyper-extended continental crust.

406 In addition to the CS1-2400 profile, we have also applied the reverse post-breakup thermal
407 subsidence modelling to the more northerly P3 and P7+11 profiles (Figure 8). Results are
408 comparable to those predicted for the CS1-2400 profile; with the proximal base salt restoring to
409 approximately sea level whilst the distal base salt restores to between 2km and 3km below global
410 sea level. Predicted thinning factors from gravity inversion, assuming normal magmatic addition, are
411 1.0 at the western end of both P3 and P7+P11 profiles consistent with the presence of oceanic crust.

412 Predicted palaeo-bathymetries for the western end of both profiles are on average 2.85km,
413 consistent with water depths on newly formed oceanic crust. For both profiles, the predicted
414 palaeo-bathymetries for base proximal salt are at or just below global sea level, while the palaeo-
415 bathymetry of base distal salt is between 2km and 3km.

416 **5. Discussion**

417 **5.1. Crustal structure and COB location**

418 Integrated quantitative analysis using gravity anomaly inversion, RDA analysis, subsidence analysis
419 and joint inversion of deep seismic reflection and gravity data have been used to determine the OCT
420 structure, COB location and magmatic type along the CS1-2400 profile, northern Angolan. Our
421 analysis shows the changes in crustal structure along profile, from which we have interpreted three
422 well defined crustal domains: oceanic crust, hyper-extended continental crust and continental crust
423 (Figure 9(a)). We have also interpreted a transitional region between the hyper-extended
424 continental crust and the start of oceanic crust. Interpretation of our results suggests that at the
425 oceanic end of the profile a normal magmatic solution is applicable, whilst at the continental end of
426 the profile a magma-starved solution is more applicable. Considering the integrated quantitative
427 analysis techniques together has enabled a robust geological interpretation of the OCT along the
428 profile to be made and a more accurate estimate the COB location to be made.

429 Our interpretation of the integrated quantitative analysis results along the CS1-2400 profile is shown
430 in Figure 9(a); our analysis suggests that:

- 431 (i) Gravity and deep seismic reflection data predict that the earliest oceanic crust is
432 approximately 5km to 7km thick.
- 433 (ii) RDA analysis shows a slightly positive sediment corrected RDA in the oceanic domain,
434 consistent with the presence of mantle dynamic uplift, which is in agreement with that
435 reported by Crosby & McKenzie (2009).

- 436 (iii) Gravity inversion, RDA analysis and subsidence analysis all suggest that both proximal and
437 distal salt is underlain by hyper-extended continental crust, not by oceanic crust.
- 438 (iv) Between the oceanic crust and the hyper-extended continental crust domain, we interpret
439 transitional crust, which we believe to be a mix of hyper-extended continental crust and
440 magmatic addition. Our interpretation of this crust is significantly different to the
441 interpretation of serpentinised exhumed mantle from Unternehr et al. (2010).
- 442 (v) Gravity anomaly inversion, RDA analysis and subsidence analysis results show that the OCT
443 along CS1-2400 is quite wide, with the distance between the COB and the margin necking
444 zone measuring approximately 180km.
- 445 (vi) Joint inversion of deep seismic reflection and gravity data shows a contrast in basement
446 density and seismic velocity between oceanic and continental crustal basement consistent
447 with our domain of transitional crust between the oceanic crust and the hyper-extended
448 crust.

449 **5.2. Palaeo-bathymetry and depositional environment of base Aptian salt**

450 Predicted palaeo-bathymetries have been determined for the base Loeme salt using 2D-flexural
451 backstripping and decompaction, together with reverse modelling of post-breakup thermal
452 subsidence. Continental lithosphere thinning factors derived from gravity anomaly inversion have
453 been used to determine the reverse post-breakup thermal subsidence. For profile CS1-2400,
454 thinning factors, derived from both the normal magmatic and magma-starved gravity inversion
455 solutions assuming a rift age of 112Ma, and used to drive the reverse post-rift thermal subsidence
456 modelling, restore the proximal autochthonous base salt to approximately 0.2km below global sea
457 level at the time of breakup. In contrast, reverse post-breakup subsidence modelling restores the
458 distal base salt to between 2km and 3km below global sea level. Similar palaeo-bathymetries for
459 base salt are also calculated for the more northerly P3 and P7+11 profiles. If we apply a continental
460 lithosphere thinning factor of 1.0 to drive the reverse post-rift thermal subsidence along the full

461 length of the three profiles (which is unreasonable), the palaeo-bathymetries of base distal salt still
462 do not restore to sea level, demonstrating that it is not possible to generate the subsidence of the
463 base salt by post-rift subsidence alone. The predicted bathymetries at breakup of the first
464 unequivocal oceanic crust are approximately 2.5km as expected for newly formed oceanic crust of
465 normal thickness. Using a rift age of 130Ma for the proximal margin increases the predicted palaeo-
466 bathymetry of base proximal salt to approximately 0.6km below global sea-level, consistent with the
467 analysis of Crosby et al. (2011).

468 Our preferred interpretation of the palaeo-bathymetric restoration of the distal and proximal base
469 salt is that all the Aptian salt was deposited between 0.2km and 0.6km below global sea level but the
470 distal salt was emplaced during late syn-rift while the continental crust under it was being actively
471 thinned resulting in additional tectonic subsidence. This is consistent with seismic evidence, which
472 shows that the distal base salt is extensionally faulted. This is also in agreement with the observation
473 by Karner and Gambôa (2007) that the rate of subsidence required to generate the accommodation
474 space for the distal salt is too large to be generated by thermal post-breakup subsidence. Crustal
475 basement thicknesses from gravity inversion, RDA and subsidence analysis, summarised in Figure 6,
476 suggest that the distal salt is underlain by hyper-extended continental crust (Figure 9(b)) rather than
477 oceanic crust or exhumed mantle as previously suggested by some authors (e.g. Reston (2010);
478 Unternehr et al. (2010)). In contrast to the distal salt, the proximal salt formed in a region where
479 crustal thinning had taken place commencing in the Neocomian or Barremian, but had ceased by the
480 upper Aptian, and is consistent with the pre-salt sag sequence under the proximal salt being post-rift
481 (Crosby et al., 2011; Unternehr et al., 2010) Our interpretation requires that the distal salt subsides
482 by syn-rift crustal thinning and post-rift thermal subsidence, whilst the proximal salt subsides by
483 post-rift thermal subsidence alone. Diachronous thinning of the continental crust from inboard to
484 outboard is to be expected from both observation and modelling ,and is consistent with breakup
485 tectonic models proposed by Péron-Pinvidic and Manatschal (2008), Pindell and Kennan (2007),
486 Ranero and Perez-Gussinye (2010) and Brune et al. (2014).

487 An alternative explanation for the different subsidence styles of proximal and distal salt has been
488 proposed by Karner and Gambôa (2007) who suggest that the sag style subsidence of proximal salt
489 but syn-tectonic style for distal salt are the result of depth-dependent lithosphere stretching and
490 thinning. While depth-dependent lithosphere stretching and thinning has been reported at rifted
491 margins (Davis and Kuszniir, 2004; Driscoll and Karner, 1998; Kuszniir and Karner, 2007), diachronous
492 rifting and thinning of the Angolan margin lithosphere from inboard to outboard may provide a
493 simpler explanation for the differing subsidence styles of proximal and distal salt.

494 An alternative interpretation is that the distal salt is para-autochthonous, and it moved down slope
495 to its present position during breakup. If in the distal regions, the salt is para-autochthonous (or
496 allochthonous) this suggests that it was not deposited in deep water and that the salt should not
497 restore to sea level. This interpretation is similar to that advocated in the Gulf of Mexico by Hudec
498 et al. (2013) and Rowan and Vendeville (2006).

499 An interpretation which is often invoked (e.g. Burke & Sengör (1988), Burke et al. (2003)) to explain
500 the palaeo-bathymetry of the base Aptian salt along the northern Angolan margin is that the distal
501 Aptian salt deposition occurred in confined environmental conditions (e.g. in a Messinian-type basin,
502 isolated from global sea level). Although a structural barrier in the south and north is not dismissed
503 (and is indeed likely), we believe that there is no definite requirement to invoke an isolated ocean
504 basin with local sea level between 2km and 3km below global sea level for the deposition of the
505 Aptian salt on the Angolan rifted margin. Furthermore our analysis suggests that both proximal and
506 distal salt on the Angolan margin are underlain by hyper-extended continental crust, not by oceanic
507 crust. The restored bathymetries of base proximal salt from this study (and also Crosby et al.
508 (2011)) are no more than 0.6km below global sea-level; a deep isolated ocean basin between 2km
509 and 3km deep for the deposition of distal salt would require a substantial difference in the depth of
510 salt deposition level, which we consider to be unlikely. A similar observation has been made by
511 Moulin et al. (2005) and Aslanian et al. (2009). Additional strong arguments against the isolated

512 basin interpretation are also presented by Pindell et al. (2014) with reference to the Gulf of Mexico;
513 they argue that an isolated basin hypothesis is unlikely as it requires a complicated scenario of inter-
514 related events to occur.

515 In summary the integrated quantitative analysis predicts the presence of oceanic crust at the
516 western end of the profile; whilst in the centre of the profile, beneath the majority of the Aptian salt
517 we interpret hyper-extended continental crust. We believe that both proximal and distal Aptian salt
518 on the Kwanza margin was deposited at a datum 0.2km to 0.6km below global sea level, but that the
519 distal salt was deposited during late syn-rift while the crust under it was being actively thinned which
520 resulted in additional tectonic subsidence. It is possible that some of the distal salt is para-
521 autochthonous and moved down-slope to its present day position. It is also possible that syn-
522 tectonic (pre-breakup) extension continued post-salt deposition in the distal region.

523

524

525

526

527

528

529

530

531

532 **6. Figure Captions**

533 **Figure 1:** Data used in the reverse post-breakup thermal subsidence modelling and gravity anomaly
534 inversion for the northern Angolan rifted continental margin. (a) Bathymetry (km) (Amante and
535 Eakins 2009), with the location of profiles CS1-2400, P3 and P7+11 indicated. (b) Satellite derived
536 free air gravity (mgal) (Sandwell and Smith 2009). (c) Deep long-offset seismic reflection depth
537 section (PSDM) for the ION CS1-2400 profile. (d) Seismic velocity model along the P3 profile
538 (Contrucci et al., 2004; Moulin et al., 2005) from seismic refraction data. (e) Seismic velocity model
539 along the P7+11 profile (Contrucci et al., 2004; Moulin et al., 2005) from seismic refraction data.

540 **Figure 2:** (a) Crustal cross section along the CS1-2400 profile, showing Moho depth from gravity
541 anomaly inversion, using the calibrated reference Moho depth of 35.5km. (b) Continental
542 lithosphere thinning profile, predicted from gravity anomaly inversion, along the CS1-2400 profile.
543 Sensitivities to a normal magmatic solution and a magma-starved solution have been examined. A
544 normal magmatic solution predicts thinning factors of 1.0 at the western end of the profile, while a
545 magma-starved solution predicts thinning factors of approximately 0.85.

546 **Figure 3:** (a) Bathymetry and depth to top basement for the CS1-2400 profile. (b) Comparison of the
547 uncorrected RDA results with the sediment corrected RDA results along the CS1-2400 profile.

548 **Figure 4:** (a) Bathymetry and depth to top basement for the CS1-2400 profile. (b) Continental
549 lithosphere thinning factors from subsidence analysis, along the CS1-2400 profile. Sensitivities to a
550 normal magmatic margin, magma-starved solution and a solution for serpentinised mantle are
551 shown.

552 **Figure 5:** (a) ION CS1-2400 PSTM deep long offset seismic profile. The horizons for seabed, top
553 basement, Moho predicted from gravity anomaly inversion and picked seismic Moho are indicated.
554 (b) Crustal cross-section along the CS1-2400 profile showing Moho depth from gravity anomaly
555 inversion, and the Moho depth determined from joint inversion; both are in good agreement, with

556 some variation in magnitude. (c) Lateral variations in basement density along the CS1-2400 profile.
557 The blue dashed line highlights the basement density of 2850kgm^{-3} which is the basement density
558 used within the initial gravity anomaly inversion. Densities range between 2770kgm^{-3} and 2970kgm^{-3} .
559 ³. (d) The corresponding lateral variations in seismic velocity along the CS1-2400 profile.

560 **Figure 6:** Summary of the integrated quantitative analysis results for the CS1-2400 profile used to
561 determine OCT structure and COB location. (a) Crustal cross section along CS1-2400 profile, with
562 Moho depth from gravity anomaly inversion. (b) The sediment corrected RDA and the RDA
563 component from variations in crustal basement thickness both have the same general trend along
564 the profile although the magnitudes differ. (c) Comparison of continental lithosphere thinning
565 factors determined using subsidence analysis and gravity anomaly inversion assuming a normal
566 magmatic solution show the same general trend along profile. (d) Smoothed crustal basement
567 densities predicted from the joint inversion of deep seismic and gravity anomaly data. (e)
568 Corresponding seismic velocities predicted from the joint inversion of deep seismic and gravity
569 anomaly data. The dashed lines indicate the interpreted boundaries between the predicted crustal
570 domains.

571 **Figure 7:** Flexural backstripping and reverse post-breakup thermal subsidence modelling along the
572 ION CS1-2400 profile. (a) Digitized present day cross section along the CS1-2400 profile; the post-salt
573 sedimentary layer is highlighted in blue; pre-salt sedimentary layer in pink; the salt layer is
574 highlighted in yellow; crust is grey and mantle is red. (b) Sediment corrected bathymetry to base salt
575 calculated from flexural backstripping and decompaction, using a T_e of 1.5km. (c) Continental
576 lithosphere thinning factor profile, from gravity anomaly inversion, for normal magmatic and
577 magma-starved solutions. (d) Reverse post-breakup thermal subsidence modelling along the CS1-
578 2400 profile, assuming a normal magmatic solution. (e) Reverse post-breakup thermal subsidence
579 modelling along the CS1-2400 profile, assuming a magma-starved solution.

580 **Figure 8:** Flexural backstripping and reverse post-breakup thermal subsidence modelling along the
581 P3 and P7+11 profiles (Contrucci et al., 2004; Moulin et al., 2005). (a) Digitized present day cross
582 section along the P3 profile; (f) Digitized present day cross section along the P7+11 profile; the post-
583 salt sedimentary layers are highlighted in turquoise, orange, green and blue; pre-salt sedimentary
584 layer in pink; the salt layer is highlighted in yellow; crust is grey and mantle is red. (b and g)
585 Sediment corrected bathymetry to base salt calculated from flexural backstripping and
586 decompaction, using a T_e of 1.5km. (c and h) Continental lithosphere thinning factors from gravity
587 anomaly inversion for a normal magmatic and a magma-starved solution. (d and i) Reverse post-
588 breakup thermal subsidence modelling along the P3 profile, assuming a normal magmatic solution.
589 (e and j) Reverse post-breakup thermal subsidence modelling along the P3 profile, assuming a
590 magma-starved solution.

591 **Figure 9:** (a) Interpretation of the integrated quantitative analysis results along the PSDM CS1-2400
592 profile. Seabed is shown in blue, top basement in green, Moho from gravity anomaly inversion in
593 black and Moho from the joint inversion is shown in pink. Our interpreted boundaries between the
594 predicted crustal domains are indicated by the dashed lines. (b) Digitized present day cross section
595 along the CS1-2400 profile; location of distal salt and proximal salt and interpreted subsidence
596 history is indicated above.

597

598 **7. References**

- 599 Alvey, A., Gaina, C., Kuszniir, N. J., and Torsvik, T. H., 2008, Integrated crustal thickness mapping and
600 plate reconstructions for the high Arctic: *Earth and Planetary Science Letters*, v. 274, no. 3-4,
601 p. 310-321.
- 602 Amante, C., and Eakins, B. W., 2009, ETOPO1 1 Arc-Minute Global Relief Model: Procedures, Data
603 Sources and Analysis: NOAA Technical Memorandum NESDIS NGDC-24, p. 19.
- 604 Aslanian, D., Moulin, M., Olivet, J.-L., Unternehr, P., Matias, L., Bache, F., Rabineau, M., Nouzé, H.,
605 Klingelhoefer, F., Contrucci, I., and Labails, C., 2009, Brazilian and African passive margins of
606 the Central Segment of the South Atlantic Ocean: Kinematic constraints: *Tectonophysics*, v.
607 468, no. 1-4, p. 98-112.
- 608 Birch, F., 1964, Density and composition of mantle and core: *Journal of Geophysical Research*, v. 69,
609 no. 20, p. 4377-4388.
- 610 Brune, S., Heine, C., Pérez-Gussinyé, M., and Sobolev, S. V., 2014, Rift migration explains continental
611 margin asymmetry and crustal hyper-extension: *Nat Commun*, v. 5.
- 612 Burke, K., MacGregor, D. S., and Cameron, N. R., 2003, Africa's petroleum systems: four tectonic
613 'Aces' in the past 600 million years: Geological Society, London, Special Publications, v. 207,
614 no. 1, p. 21-60.
- 615 Burke, K., and Sengör, A. M. C., 1988, Ten metre global sea-level change associated with South
616 Atlantic Aptian salt deposition: *Marine Geology*, v. 83, no. 1-4, p. 309-312.
- 617 Carlson, R. L., and Herrick, C. N., 1990, Densities and porosities in the oceanic crust and their
618 variations with depth and age: *Journal of Geophysical Research: Solid Earth*, v. 95, no. B6, p.
619 9153-9170.
- 620 Carlson, R. L., and Raskin, G. S., 1984, Density of the ocean crust: *Nature*, v. 311, no. 5986, p. 555-
621 558.
- 622 Chappell, A. R., and Kuszniir, N. J., 2008, Three-dimensional gravity inversion for Moho depth at rifted
623 continental margins incorporating a lithosphere thermal gravity anomaly correction:
624 *Geophysical Journal International*, v. 174, no. 1, p. 1-13.
- 625 Christensen, N. I., and Mooney, W. D., 1995, Seismic velocity structure and composition of the
626 continental crust: A global view: *Journal of Geophysical Research: Solid Earth*, v. 100, no. B6,
627 p. 9761-9788.
- 628 Contrucci, I., Matias, L., Moulin, M., Géli, L., Klingelhoefer, F., Nouzé, H., Aslanian, D., Olivet, J.-L.,
629 Réhault, J.-P., and Sibuet, J.-C., 2004, Deep structure of the West African continental margin
630 (Congo, Zaïre, Angola), between 5°S and 8°S, from reflection/refraction seismics and gravity
631 data: *Geophysical Journal International*, v. 158, no. 2, p. 529-553.
- 632 Cowie, L., 2015, Determination of Ocean Continent Transition Structure, Continent Ocean Boundary
633 Location and Magmatic Type at Rifted Continental Margins [PhD: University of Liverpool, 280
634 p.
- 635 Cowie, L., and Kuszniir, N., 2012, Mapping crustal thickness and oceanic lithosphere distribution in
636 the Eastern Mediterranean using gravity inversion: *Petroleum Geoscience*, v. 18, no. 4, p.
637 373-380.
- 638 Crosby, A. G., and McKenzie, D., 2009, An analysis of young ocean depth, gravity and global residual
639 topography: *Geophysical Journal International*, v. 178, no. 3, p. 1198-1219.
- 640 Crosby, A. G., White, N. J., Edwards, G. R. H., Thompson, M., Corfield, R., and Mackay, L., 2011,
641 Evolution of deep-water rifted margins: Testing depth-dependent extensional models:
642 *Tectonics*, v. 30, no. 1, p. n/a-n/a.
- 643 Davis, M., and Kuszniir, N., 2004, Depth Dependant lithospheric Stretching at Rifted Continental
644 Margins, *in* Karner, G. D., Taylor, B., Driscoll, N. W., and Kohlstedt, D. L., eds., *Rheology and
645 Deformation of the Lithosphere at Continental Margins*, Columbia University Press, p. 408.

646 Dean, S. M., Minshull, T. A., Whitmarsh, R. B., and Louden, K. E., 2000, Deep structure of the ocean-
647 continent transition in the southern Iberia Abyssal Plain from seismic refraction profiles: The
648 IAM-9 transect at 40°20'N: *Journal of Geophysical Research: Solid Earth*, v. 105, no. B3, p.
649 5859-5885.

650 Discovery 215 Working, G., Minshull, T. A., Dean, S. M., Whitmarsh, R. B., Russell, S. M., Louden, K.
651 E., and Chian, D., 1998, Deep structure in the vicinity of the ocean-continent transition zone
652 under the southern Iberia Abyssal Plain: *Geology*, v. 26, no. 8, p. 743-746.

653 Driscoll, N. W., and Karner, G. D., 1998, Lower crustal extension across the Northern Carnarvon
654 basin, Australia: Evidence for an eastward dipping detachment: *Journal of Geophysical
655 Research: Solid Earth*, v. 103, no. B3, p. 4975-4991.

656 Fowler, C. M. R., 2006, *The Solid Earth: An Introduction to Global Geophysics*, Cambridge University
657 Press, 685 p.:

658 Greenhalgh, E. E., and Kuszniir, N. J., 2007, Evidence for thin oceanic crust on the extinct Aegir Ridge,
659 Norwegian Basin, NE Atlantic derived from satellite gravity inversion: *Geophysical Research
660 Letters*, v. 34, no. 6, p. L06305.

661 Hudec, M. R., and Jackson, M. P. A., 2007, Terra infirma: Understanding salt tectonics: *Earth-Science
662 Reviews*, v. 82, no. 1-2, p. 1-28.

663 Hudec, M. R., Norton, I. O., Jackson, M. P. A., and Peel, F. J., 2013, Jurassic Evolution of the Gulf of
664 Mexico Salt Basin: *AAPG Bulletin*, v. 97, no. 1, p. 1683 - 1710.

665 Jackson, M. P. A., Cramez, C., and Fonck, J.-M., 2000, Role of subaerial volcanic rocks and mantle
666 plumes in creation of South Atlantic margins: implications for salt tectonics and source
667 rocks: *Marine and Petroleum Geology*, v. 17, no. 4, p. 477-498.

668 Karner, G. D., and Driscoll, N. W., 1999, Tectonic and stratigraphic development of the West African
669 and eastern Brazilian Margins: insights from quantitative basin modelling: *Geological
670 Society, London, Special Publications*, v. 153, no. 1, p. 11-40.

671 Karner, G. D., Driscoll, N. W., and Barker, D. H. N., 2003, Syn-rift regional subsidence across the West
672 African continental margin: the role of lower plate ductile extension: *Geological Society,
673 London, Special Publications*, v. 207, no. 1, p. 105-129.

674 Karner, G. D., Driscoll, N. W., McGinnis, J. P., Brumbaugh, W. D., and Cameron, N. R., 1997, Tectonic
675 significance of syn-rift sediment packages across the Gabon-Cabinda continental margin:
676 *Marine and Petroleum Geology*, v. 14, no. (7-8), p. 973-1000.

677 Karner, G. D., and Gambôa, L. A. P., 2007, Timing and origin of the South Atlantic pre-salt sag basins
678 and their capping evaporites: *Geological Society, London, Special Publications*, v. 285, no. 1,
679 p. 15-35.

680 Kuszniir, N. J., and Karner, G. D., 2007, Continental lithospheric thinning and breakup in response to
681 upwelling divergent mantle flow: application to the Woodlark, Newfoundland and Iberia
682 margins: *Geological Society, London, Special Publications*, v. 282, no. 1, p. 389-419.

683 Kuszniir, N. J., Roberts, A. M., and Morley, C. K., 1995, Forward and reverse modelling of rift basin
684 formation: *Geological Society, London, Special Publications*, v. 80, no. 1, p. 33-56.

685 Le Pichon, X., and Sibuet, J.-C., 1981, Passive margins: A model of formation: *Journal of Geophysical
686 Research: Solid Earth*, v. 86, no. B5, p. 3708-3720.

687 Ludwig, W. J., Nafe, J. E., and C. L. Drake, A. E., 1970, Seismic refraction, in *The Sea*, Wiley-
688 Interscience, 53-84 p.:

689 Manatschal, G., Froitzheim, N., Rubenach, M., and Turrin, B. D., 2001, The role of detachment
690 faulting in the formation of an ocean-continent transition: insights from the Iberia Abyssal
691 Plain: *Geological Society, London, Special Publications*, v. 187, no. 1, p. 405-428.

692 Manatschal, G., Sutra, E., and Péron-Pinvidic, G., The lesson from the Iberia-Newfoundland rifted
693 margins: how applicable is it to other rifted margins?, in *Proceedings 2nd Central & North
694 Atlantic Conjugate Margins: Rediscovering the Atlantic, New Insights, New winds for an old
695 sea2010, Volume 2*, p. 27 - 37.

696 McKenzie, D., 1978, Some Remarks on the Development of Sedimentary Basins Earth and Planetary
697 Science Letters, v. 40, p. 25-32.

698 Moulin, M., 2003, Etude géologique et géophysique des marges continentales passives: exemple du
699 Zaire et de l'Angola [PhD: University de Bretagne Occidentale, 360 p.

700 Moulin, M., Aslanian, D., Olivet, J.-L., Contrucci, I., Matias, L., Géli, L., Klingelhoefer, F., Nouzé, H.,
701 Réhault, J.-P., and Unternehr, P., 2005, Geological constraints on the evolution of the
702 Angolan margin based on reflection and refraction seismic data (ZaiAngo project):
703 Geophysical Journal International, v. 162, no. 3, p. 793-810.

704 Müller, R. D., Roest, W. R., Royer, J.-Y., Gahagan, L. M., and Sclater, J. G., 1997, Digital isochrons of
705 the world's ocean floor: Journal of Geophysical Research, v. 102, no. B2, p. 3211-3214.

706 Müller, R. D., Sdrolias, M., Gaina, C., Steinberger, B., and Heine, C., 2008, Long-Term Sea-Level
707 Fluctuations Driven by Ocean Basin Dynamics: Science, v. 319, no. 5868, p. 1357-1362.

708 Parker, R. L., 1972, The Rapid Calculation of Potential Anomalies: Geophysical Journal of the Royal
709 Astronomical Society, v. 31, no. 4, p. 447-455.

710 Parsons, B., and Sclater, J. G., 1977, An Analysis of the Variation of Ocean Floor Bathymetry and Heat
711 Flow with Age: Journal of Geophysical Research, v. 82, no. 5, p. 803-827.

712 Péron-Pinvidic, G., and Manatschal, G., 2008, The final rifting evolution at deep magma-poor passive
713 margins from Iberia-Newfoundland: a new point of view: International Journal of Earth
714 Sciences, v. 98, no. 7, p. 1581-1597.

715 Péron-Pinvidic, G., Manatschal, G., Minshull, T. A., and Sawyer, D. S., 2007, Tectonosedimentary
716 evolution of the deep Iberia-Newfoundland margins: Evidence for a complex breakup
717 history: Tectonics, v. 26, no. 2, p. TC2011.

718 Pindell, J. L., and Kennan, L., 2007, Rift models and the salt-cored marginal wedge in the northern
719 Gulf of Mexico: implications for deep water paleogene Wilcox deposition and basinwide
720 maturation: Transactions of GCSSEPM 27th Annual Bob F. Perkins Research Conference, p.
721 146-186.

722 Ranero, C. R., and Perez-Gussinye, M., 2010, Sequential faulting explains the asymmetry and
723 extension discrepancy of conjugate margins: Nature, v. 468, no. 7321, p. 294-299.

724 Reston, T. J., 2010, The opening of the central segment of the South Atlantic: symmetry and the
725 extension discrepancy: Petroleum Geoscience, v. 16, no. 3, p. 199-206.

726 Roberts, A. M., Corfield, R. I., Kuszniir, N. J., Matthews, S. J., Hansen, E.-K., and Hooper, R. J., 2009,
727 Mapping palaeostructure and palaeobathymetry along the Norwegian Atlantic continental
728 margin: Møre and Vøring basins: Petroleum Geoscience, v. 15, no. 1, p. 27-43.

729 Roberts, A. M., Kuszniir, N. J., Corfield, R. I., Thompson, M., and Woodfine, R., 2013, Integrated
730 tectonic basin modelling as an aid to understanding deep-water rifted continental margin
731 structure and location: Petroleum Geoscience, v. 19, no. 1, p. 65-88.

732 Roberts, A. M., Kuszniir, N. J., Yielding, G., and Styles, P., 1998, 2D flexural backstripping of
733 extensional basins; the need for a sideways glance: Petroleum Geoscience, v. 4, no. 4, p.
734 327-338.

735 Rowan, M. G., and Vendeville, B. C., 2006, Foldbelts with early salt withdrawal and diapirism:
736 Physical model and examples from the northern Gulf of Mexico and the Flinders Ranges,
737 Australia: Marine and Petroleum Geology, v. 23, no. 9-10, p. 871-891.

738 Sandwell, D. T., and Smith, W. H. F., 2009, Global marine gravity from retracked Geosat and ERS-1
739 altimetry: Ridge segmentation versus spreading rate: Journal of Geophysical Research, v.
740 114, no. B1, p. B01411.

741 Sclater, J. G., and Christie, P. A. F., 1980, Continental stretching: An explanation of the Post-Mid-
742 Cretaceous subsidence of the central North Sea Basin: Journal of Geophysical Research: Solid
743 Earth, v. 85, no. B7, p. 3711-3739.

744 Stein, C. A., and Stein, S., 1992, A model for the global variation in oceanic depth and heat flow with
745 lithospheric age: Nature, v. 359, no. 6391, p. 123-129.

746 Teisserenc, P., and Villemin, J., 1989, Sedimentary basin of Gabon – geology and oil systems, *in*
747 Edwards, J. D., and Santogrossi, P. A., eds., *Divergent / Passive Margin Basins*. Memoir of the
748 American Association of Petroleum Geologists, Volume 48.
749 Unternehr, P., Péron-Pinvidic, G., Manatschal, G., and Sutra, E., 2010, Hyper-extended crust in the
750 South Atlantic: in search of a model: *Petroleum Geoscience*, v. 16, no. 3, p. 207-215.
751 White, R., and McKenzie, D., 1989, Magmatism at Rift Zones: The Generation of Volcanic Continental
752 Margins and Flood Basalts: *Journal of Geophysical Research*, v. 94, no. B6, p. 7685-7729.
753 Whitmarsh, R. B., and Miles, P. R., 1995, Models of the development of the West Iberia rifted
754 continental margin at 40°30'N deduced from surface and deep-tow magnetic anomalies:
755 *Journal of Geophysical Research: Solid Earth*, v. 100, no. B3, p. 3789-3806.

756

757

758

759

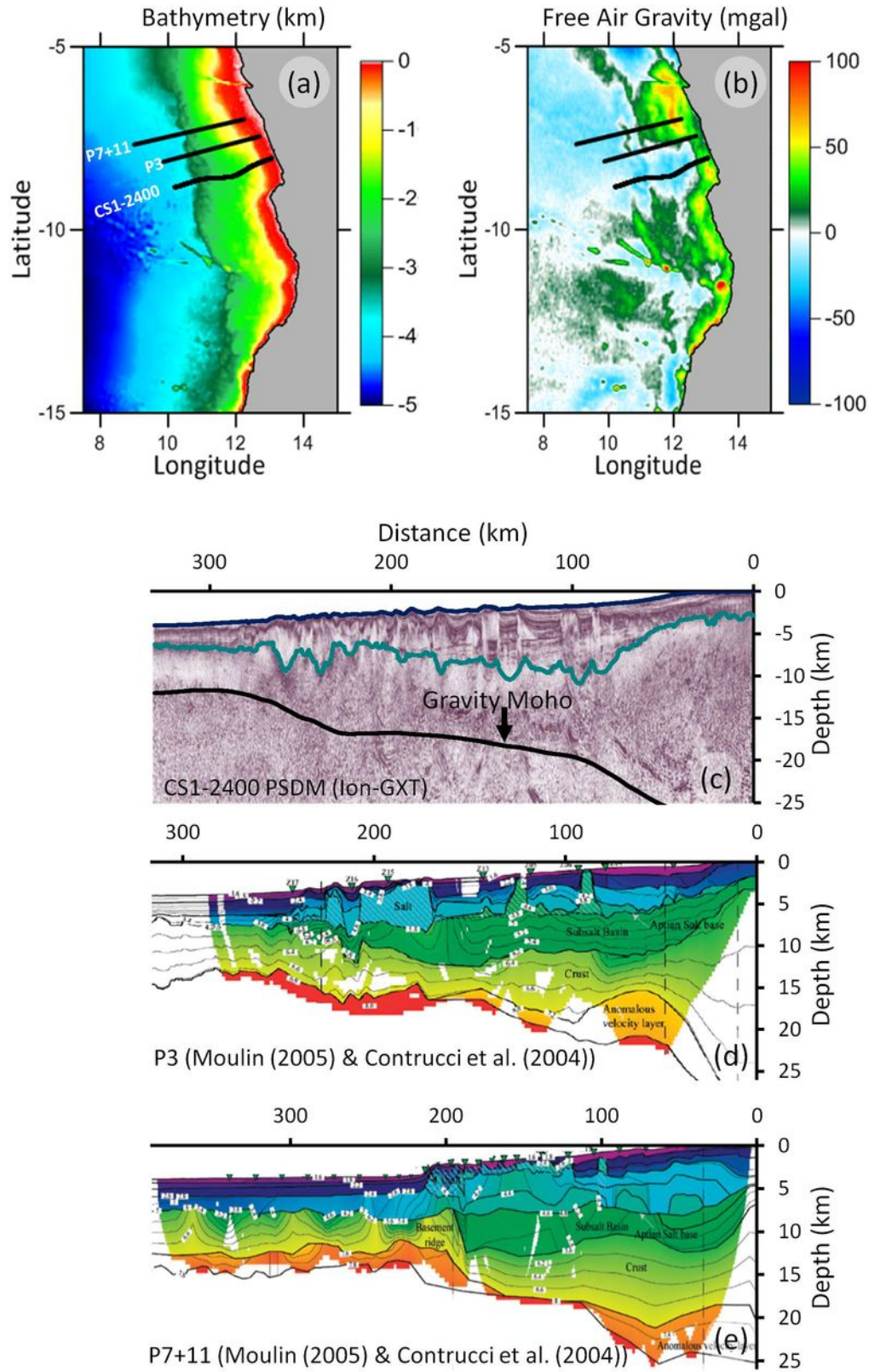
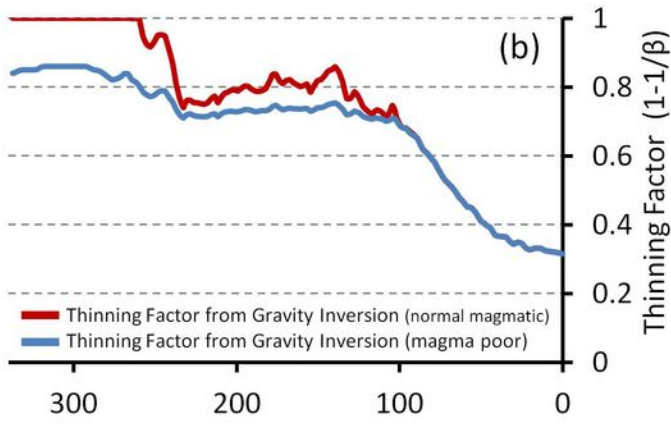
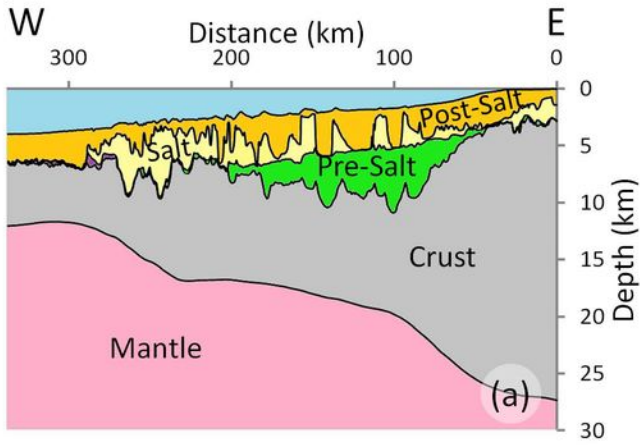
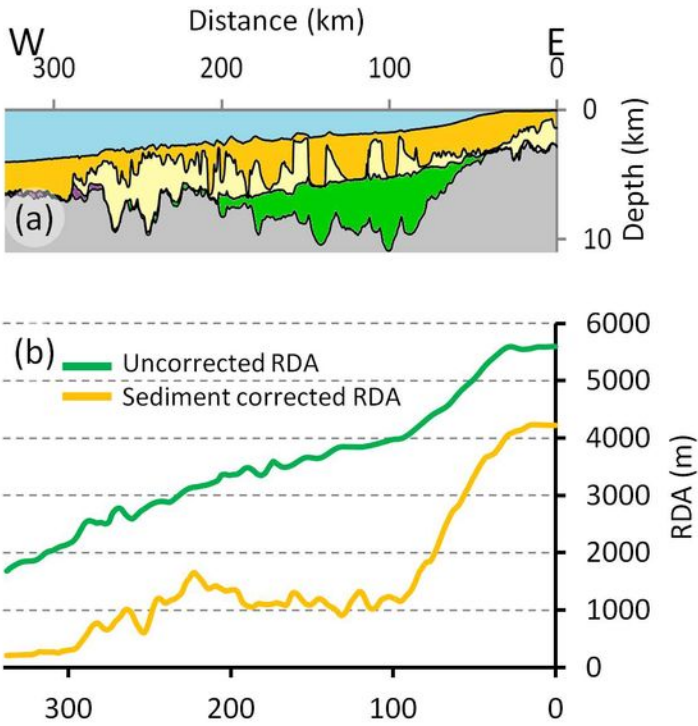
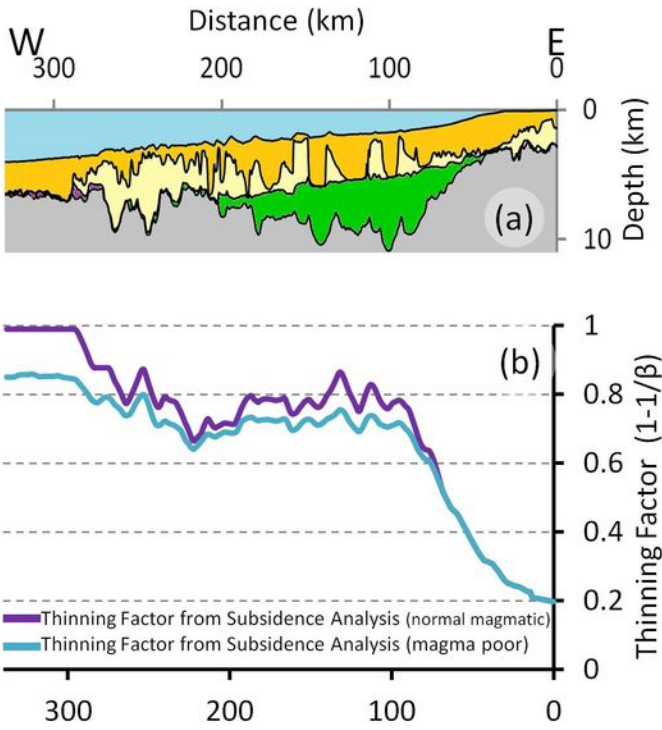


Figure 2

Cowie, Angelo, Kuszniir, Manatschal & Horn 2014







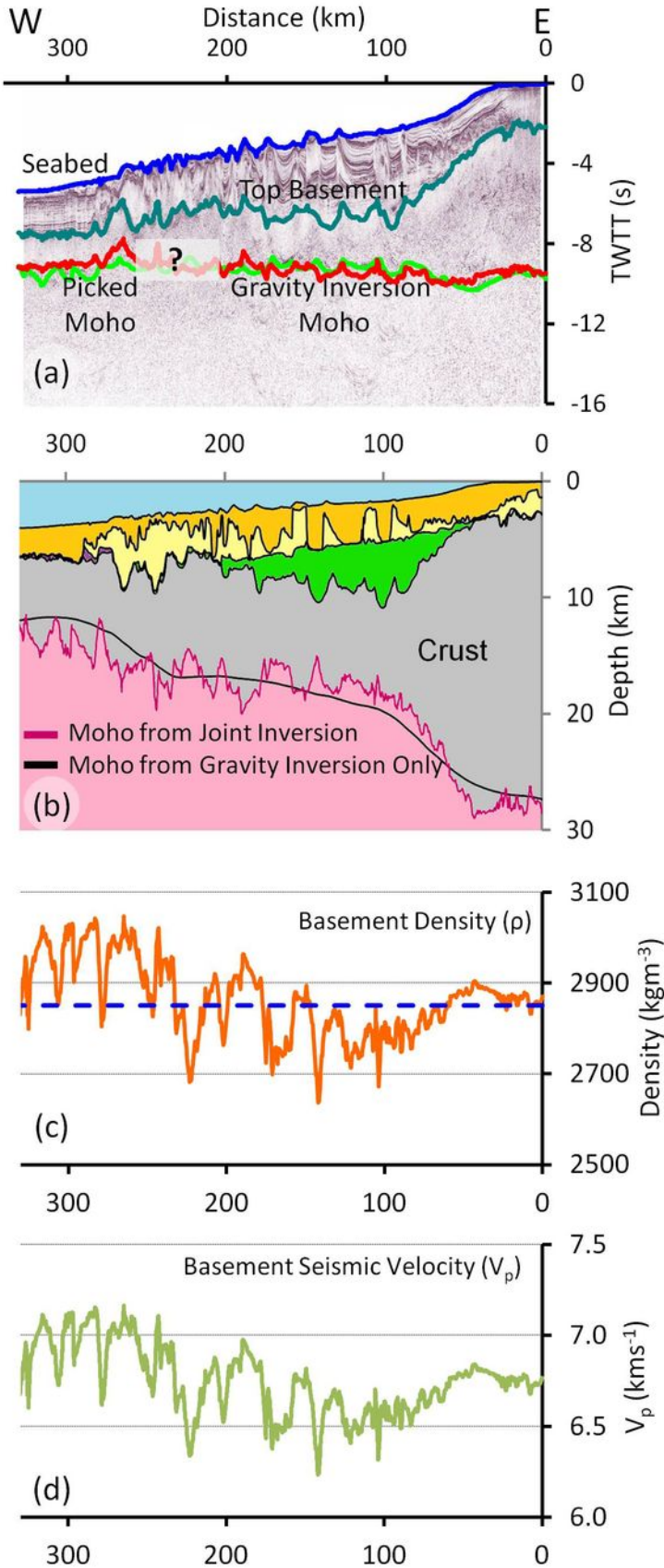
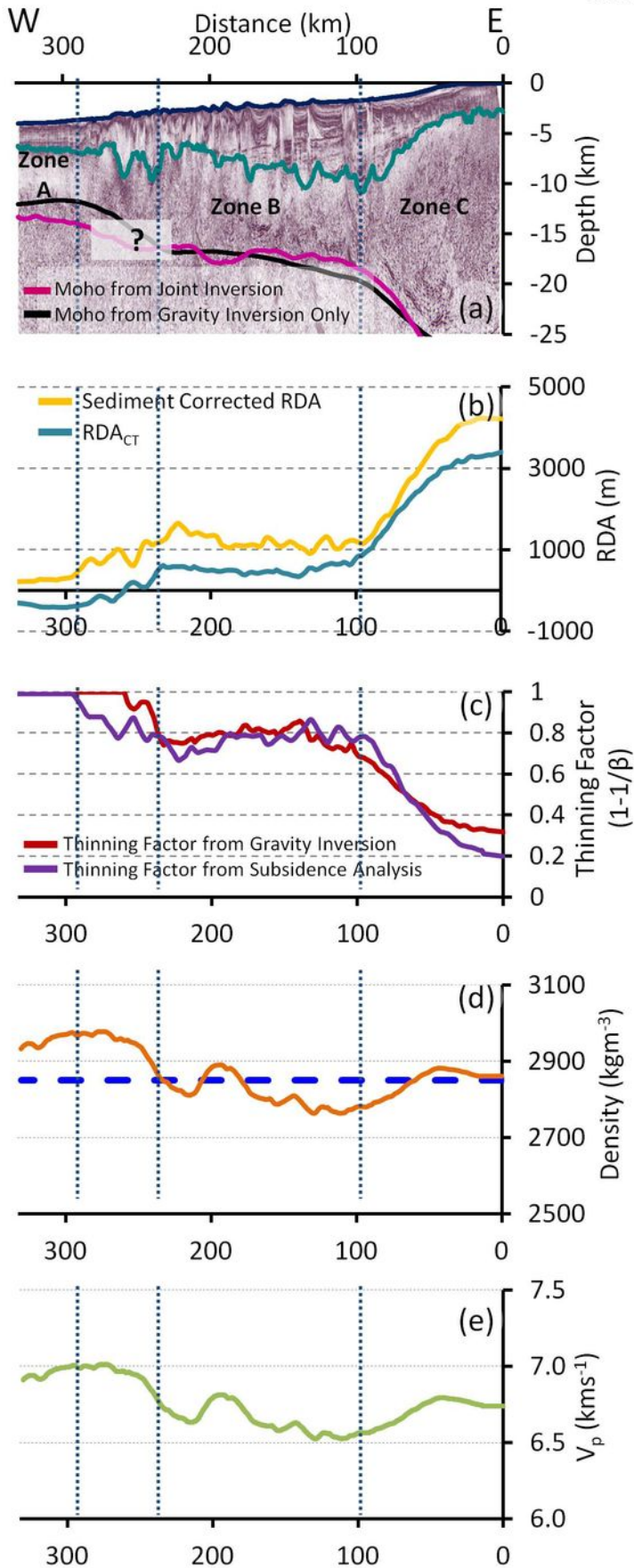
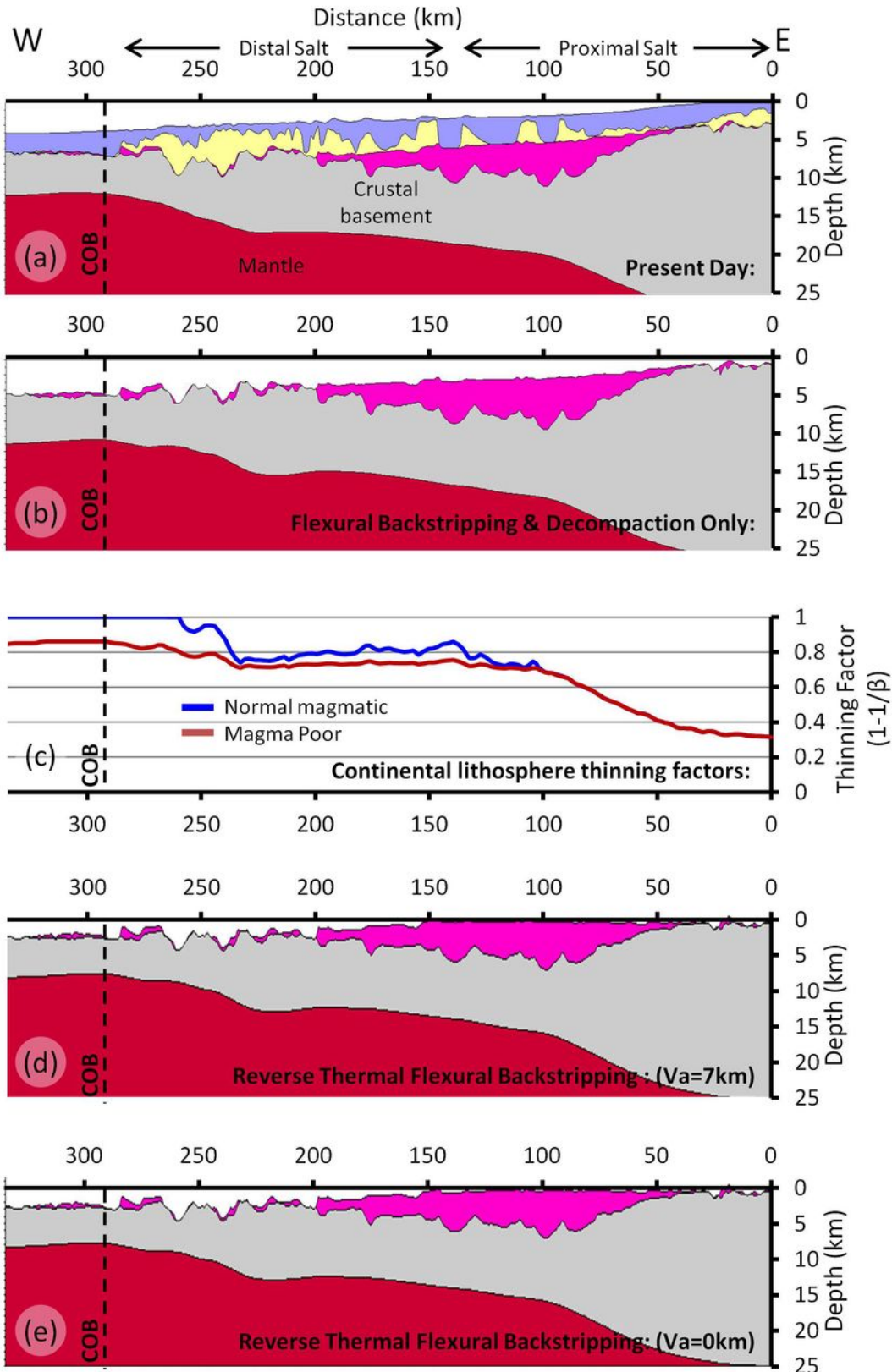


Figure 6

Cowie, Angelo, Kuszniir, Manatschal & Horn 2014



ION-GXT CS1-2400 profile:



P3 profile: (Moulin (2003) & Contrucci et al., (2004))

P7+11 profile (Moulin (2003) & Contrucci et al., (2004))

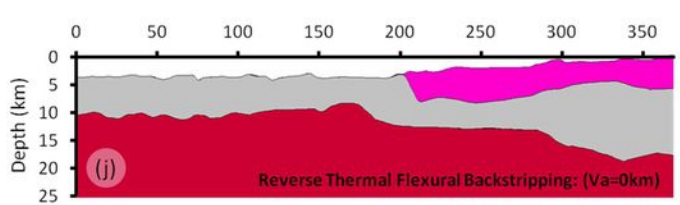
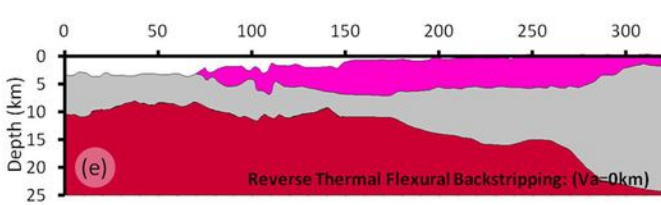
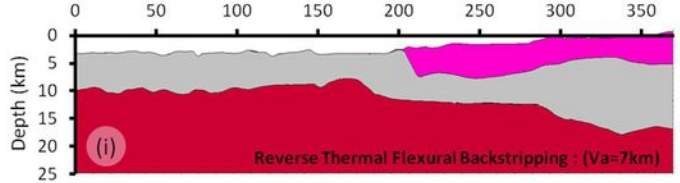
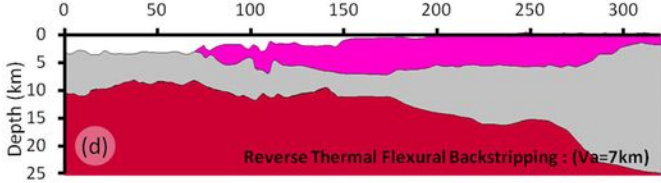
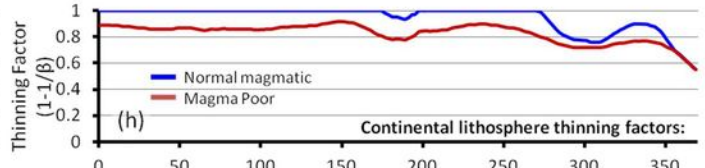
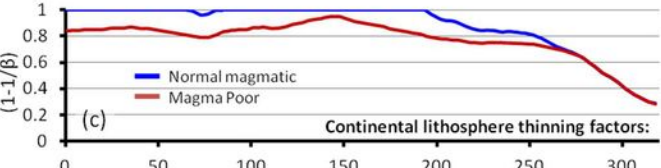
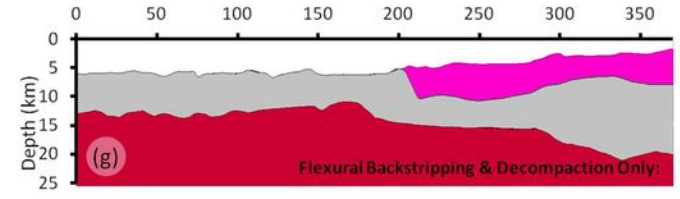
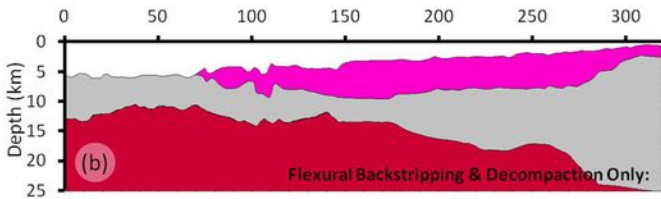
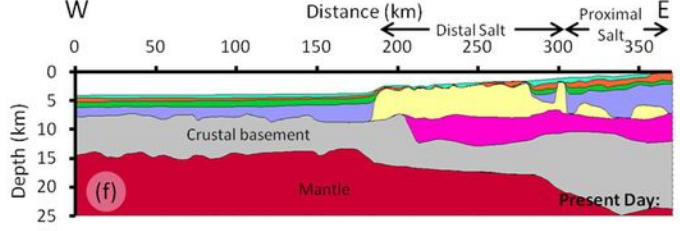
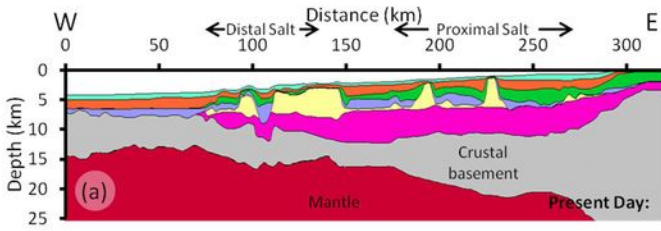


Figure 9

Cowie, Angelo, Kuszniir, Manatschal & Horn 2014

